HHS Public Access

Author manuscript

*Ultrasound Med Biol*. Author manuscript; available in PMC 2018 October 01.

Published in final edited form as:

*Ultrasound Med Biol*. 2017 October ; 43(10): 2302–2317. doi:10.1016/j.ultrasmedbio.2017.06.010.

# Effect of Frequency and Focal Spacing on Transcranial Histotripsy Clot Liquefaction Using Electronic Focal Steering

**Tyler Gerhardson**[1], **Jonathan R. Sukovich**[1], **Aditya S. Pandey**[2], **Timothy L. Hall**[1], **Charles A. Cain**[1], and **Zhen Xu**[1,3]

[1]Department of Biomedical Engineering, University of Michigan, Ann Arbor, MI, USA

[2]Department of Neurological Surgery, University of Michigan, Ann Arbor, MI, USA

[3]Department of Pediatrics and Communicable Diseases, University of Michigan, Ann Arbor, MI, USA

## Abstract

This *in-vitro* study investigated the effects of ultrasound frequency and focal spacing on blood clot liquefaction via transcranial histotripsy. Histotripsy pulses were delivered using two 256-element hemispherical transducers of different frequency (250 and 500 kHz) with 30 cm aperture diameters. A 4 cm diameter spherical volume of *in-vitro* blood clot was treated through three excised human skullcaps by electronically steering the focus with frequency proportional focal spacing: λ/2, 2λ/3 and λ with 50 pulses per location. The pulse repetition frequency (PRF) across the volume was 200 Hz, corresponding to a duty cycle of 0.08% (250 kHz) and 0.04% (500 kHz) for each focal location. Skull heating during treatment was monitored. Liquefied clot was drained via catheter and syringe in range of 6–59 mL in 0.9–42.4 minutes. The fastest rate was 16.6 mL/min. The best parameter combination was λ spacing at 500 kHz which produced large liquefaction through three skullcaps (23.1 ± 4.0, 37.1 ± 16.9 and 25.4 ± 16.9 mL) with the fast rates (3.2 ± 0.6, 5.1 ± 2.3 and 3.5 ± 0.4 mL/min). The temperature rise through the 3 skullcaps remained below 4 °C.

### Keywords

Histotripsy; Intracerebral Hemorrhage; Hemorrhagic Stroke; Electronic Focal Steering; Cavitation

## Introduction

Intracerebral hemorrhage (ICH) accounts for 10–15% of all strokes and affects approximately two million people worldwide (Qureshi et al. 2009; Kulina et al. 2012; Go et al. 2013). ICH is characterized by blood vessel rupture within the brain that leads to the

Corresponding Author: Tyler Gerhardson, University of Michigan, Department of Biomedical Engineering, 2200 Bonisteel Blvd, Ann Arbor, MI 48109, USA., Phone: (413) 265-9862, tgerhard@umich.edu.

formation of a blood clot therein. Due to its encasement by the skull, the formation of a blood clot within the brain causes an increase in intracranial pressure that can cause immediate injury to neurons and axons via mechanical distortion. In addition, the rise in intracranial pressures (ICP) and brain swelling leads to secondary injuries that can occur as the cerebral perfusion pressure (CCP) decreases. The extent of the ICP increase is dependent on the size of the ICH and is a significant factor in patient outcome. Further, delayed cerebral toxicity is caused by the degradation of remaining blood products. In general, patients diagnosed with ICH have a 30-day mortality rate of approximately 40% (Flaherty et al. 2006). Large clots (30 to 60 mL) are even more detrimental to patient outcome (Broderick et al. 1993; Broderick et al. 1994; Dennis 2003; Flaherty et al. 2006). This necessitates a fast and effective evacuation procedure for blood clots formed within the brain. The mainstay treatment for ICH is surgical evacuation via a craniotomy. Craniotomy provides a quick access to evacuate clots; however, the procedure remains highly invasive as normal brain tissue may need to be traversed to remove the clots. In fact, craniotomy surgery leading to removal of ICH has not been shown to improve the functional outcome or reduce the morbidity and this lack of effectiveness may be related to the injury caused to surrounding cerebral tissue (Hankey and Hon 1997; Fernandes et al. 2000; Mendelow et al. 2005; Mendelow et al. 2013).

Minimally invasive clot evacuation techniques have been developed to overcome the issues associated with craniotomy-based surgeries. Specifically, techniques using a catheter inserted through a small hole in the skull to deliver thrombolytic drugs, such as recombinant tissue plasminogen activator (rt-PA), to liquefy clots and aspirate the liquefied volume have been investigated. However, due to the slow perfusion of the thrombolytic drugs into the clot, the treatment typically takes 3–7 days with the catheter within the ICH for the entire duration thus requiring a lengthy intensive care unit (ICU) stay. These techniques are currently undergoing clinical investigation with early results revealing an ability to reduce clot size as well as ICH related edema (Hattori et al. 2006; Morgan et al. 2008; Wang et al. 2009). However, the functional outcome of ICH survivors has not improved, likely due to the long treatment time required to liquefy and aspirate the volume. Additionally, although such techniques have reported up to a 50% reduction in clot size, this may not be sufficient for large clots, where a greater reduction may be necessary and cause treatment times to exceed what is clinically feasible (i.e., > 7 days). For smaller clots typical of ischemic stroke, thrombolytic drugs, such as rt-PA, have been administered with and without contrast agent microbubbles and clots have been insonated with low-amplitude ultrasound pulses to increase the efficacy and rate of clot liquefaction (Alexandrov et al. 2004; Datta et al. 2006; Holland et al. 2008; Hitchcock and Holland 2010; Meairs et al. 2012). The combination of microbubbles and ultrasound has shown improved penetration of thrombolytic drugs into clots (Datta et al. 2008). Although such increased penetration may be sufficient for treating smaller clots found with ischemic stroke, the penetration depth may still be a limiting factor for larger clots typical of ICH.

High intensity focused ultrasound (HIFU) techniques have been investigated for various brain applications. Magnetic resonance guided focused ultrasound (MRgFUS) is one particular technique that uses a thermal mechanism to deliberately kill tissue at a precise focal point and MR imaging to correct for the acoustic aberration and monitor the efficacy of

the treatment. MRgFUS has established itself as a transcranial therapy and has had success in treating single spots in the brain for movement disorders such as essential tremor (Elias et al. 2013a, Elias et al. 2013b). MRgFUS has also been used to enhance drug delivery through blood brain barrier for treatment of brain tumors (Hynynen et al. 2006a; O'Reilly and Hynynen 2012; Nance et al. 2014). In addition, MRgFUS has been shown to thermally lyse clots through the skull in animal and human cadaver studies by increasing the temperature of the target clot by approximately 6 °C which is thought to cause mechanical breakdown of the clot via inertial cavitation (Monteith et al. 2013a; Monteith et al. 2013b). The resulting liquid can then be aspirated out with a drainage catheter inserted through a bur hole in the skull. This provides a minimally invasive alternative for ICH treatment that does not use thrombolytic drugs and provides much faster liquefaction than the current clinical treatments. However, due to skull overheating caused by the applied ultrasound (≥100 μs at 10% duty cycle), MRgFUS has not been able to treat clots greater than 40 mL or regions within 2 cm of the skull, thus excluding ~80% of the brain cortex region where clots can form (Monteith et al. 2013a; Monteith et al. 2013c; Wright et al. 2012; Ramanan and Shankar 2013). Additionally, although MRgFUS has shown the capacity to accelerate clot reduction time (3 hours to liquefy up to 40 mL), the treatment time is still long relative to that needed for critical cases (i.e., patients with clots greater than 60 mL).

Histotripsy is another FUS technology currently being developed for ICH treatment. Histotripsy uses short (≤ 2 cycles or ≤ 4μs at 500kHz), high energy pulses at a very low duty cycle (< 0.1%) to generate cavitation microbubble clouds transcranially using the intrinsic threshold method. In this method, cavitation is generated with the peak-negative pressure directly exceeding the threshold intrinsic to the target media to excite the pre-existing nuclei in the target tissue (Xu et al. 2004; Xu et al. 2005; Roberts et al. 2006; Xu et al. 2010). In water based tissues such as clots this threshold is about 27 MPa with little change expected at different frequencies (Vlaisavljevich et al. 2015a). The rapid and energetic bubble expansion and collapse of cavitation create high stress and strain in the clot at the focus that fractionates it into an acellular homogenate (Lin et al. 2014). In contrast to other FUS techniques, the tissue destruction caused by histotripsy has been shown to be purely mechanical, with negligible thermal effects (Kieran et al. 2007). Histotripsy clot liquefaction has been demonstrated in deep vein thrombosis model both *in-vitro* and *in-vivo* (Maxwell et al. 2009; Maxwell et al. 2011). Recently, histotripsy and boiling histotripsy have been used for treatment in an *in-vitro* large extravascular hematoma model (Khokhlova et al. 2016). Additionally, the *in-vitro* feasibility of histotripsy as a transcranial therapy for brain tissue has been investigated (Kim et al. 2014; Sukovich et al. 2016).

Similar to MRgFUS, histotripsy can be used to liquefy clot through the skull, and the liquefied clot volume can be drained via a catheter inserted into the clot through a small burr hole. By using extremely short pulses (microsecond duration) and a low duty cycle (≤0.1%) to minimize skull heating, we hypothesize that histotripsy can overcome the limitations of MRgFUS to accelerate the treatment speed, widen the treatment location range to regions closer to the skull surface, and liquefy clots larger than 40 mL.

In this paper, the use of histotripsy with electronic focal steering for fast transcranial clot liquefaction is demonstrated. The specific emphasis was to analyze the effects of transducer

frequency and focal spacing on treatment efficacy and speed. Frequency is an important treatment parameter as attenuation through the skull, lesion size and electronic focal steering range are all factors affected by the frequency of the applied treatment. Likewise, the focal spacing is another significant treatment parameter as the spacing between individual points in a given treatment region affects the overall lesion, the number of treatment points and thus treatment speed. Frequency and focal spacing were chosen as the studied variables as it was expected that these variables had the largest potential to significantly reduce treatment time for the treatment of a given volume of clot. By making the focal spacing proportional to frequency and studying the effects of frequency and focal spacing we were able analyze treatment across a large range of treatment times. In addition, because the skull is highly absorbing and skull heating is a major issue limiting transcranial ultrasound therapy, the temperature rise in the skull during histotripsy treatment was measured.

## Methods

### Phased Array Histotripsy Transducers

Two different 256-element hemispherical ultrasound transducer arrays both with 15 cm focal distance were used in this study. The center frequencies were 250 kHz and 500 kHz. The arrays were built in-house according to methods similar to those described in (Kim et al. 2014). The transducer elements populating the array were comprised of two 20 mm diameter flat, stacked piezo ceramic (PZ36) disc elements. The 256 transducer elements were used to populate a hemispherical scaffold, filling the entirety of the scaffold except for the most central region of the scaffold, in which there were no elements. Each transducer array was positioned into a tank of degassed water at room temperature. A 256-channel high voltage pulser capable of delivering short bursts was used to drive the elements of each array. The timing of the pulsers was controlled by a custom digital signal generator programmed through MATLAB (MathWorks, Natick, MA, USA) allowing independent control of each element of the array and the generation of complex synchronized pulsing patterns. The transducer was calibrated using a fiber optic hydrophone (FOPH) built in-house (Parsons et al. 2006). For measurements above the intrinsic threshold, cavitation exists 100% of the time and peak-negative pressures near or beyond 27 MPa cannot be measured. However, as the calibrations were performed in degassed water, there is a low probability of the occurrence of “incidental cavitation bubbles” in this media at pressures above 20 MPa (Vlaisavljevich et al. 2015a). Therefore, peak-negative pressure measurements beyond 20 MPa reported throughout this paper are estimated by linear summation of the peak-negative pressure amplitudes output by subsets of the individual transducer elements. This linear summation pressure extrapolation technique is only intended to serve as an indication of the probability of cavitation activity in the focal region and the *potential* pressure overhead available during treatment and not an accurate estimate of pressure *in situ*.

### Sample Preparation

**Skullcap Preparation—**In all experiments, histotripsy was applied to the target blood clot through an excised human skullcap in a degassed water tank. To analyze the variation in clot liquefaction across skullcaps, three excised human skullcaps obtained through the University of Michigan Anatomical Donations Program were used for each transducer frequency and

focal spacing combination. The skullcaps were defleshed and cleaned after extraction and continuously kept in either water or a bleach-water solution of up to a 5% concentration thereafter. The bleach was added to keep algae or bacteria from growing on the surface of the skullcap and the walls of the storage container. This accumulation of algae was noticed during storage of skulls during the duration of the 500 kHz treatments and the water required frequent replacement. The bleach-water storage solution was implemented around the time which the 250 kHz experiments began. Prior to experiments, the skullcaps were degassed inside a vacuum chamber for a minimum of one week. The measured dimensions and acoustic properties of the three skullcaps used in these experiments can be found in Table 1. The thickness, long and short axis and depth dimensions of the skullcaps were measured using 3D laser scans (Ultra HD 2020i, NextEngine, Santa Monica, California) of each skullcap. Attenuation and sound speed measurements were obtained by using a PVDF capsule hydrophone (HGL200, Onda, Sunnyvale, CA, USA) to measure the pressure and time of flight from individual elements of each array with and without the skullcap concentrically placed within the array. Using the 3D laser scans of each skullcap, the skullcap was mapped into 256 discrete thickness values that corresponded to the region of skull centered around the ray from each element. The attenuation was calculated using the decrease in peak negative pressure due to the presence of the skullcap. The speed of sound was calculated from the change in arrival time due to the presence of the skullcap.

**Red Blood Cell (RBC) Phantom Preparation—**RBC phantoms were used to analyze the lesion generation with electronic focal steering through excised human skullcaps. Phantoms were prepared from an agarose-saline mixture and RBCs according protocols previously established by our lab (Maxwell et al. 2010). These phantoms consisted of three layers: a thin (~500 μm) RBC-agarose gel layer between two thicker (~10 mm) transparent agarose gel layers. As the RBC-agarose gel layer changed from translucent and red to transparent and colorless following the destruction of the RBC layer that resulted from cavitation, the phantom provided good contrast for visualizing cavitation damage.

**Blood Clot Preparation—**In vitro blood clots of 5 cm in diameter were made with bovine blood harvested from a local abattoir. Upon harvesting, the blood mixed with citrate phosphate dextrose (CPD) (Boston Bioproducts, Ashland, MA, USA) with a CPD-to-blood ratio of 1:9 (v:v) to prevent it from clotting. The blood was stored at 4 °C prior to use. All blood was used within two weeks of harvesting. 78 mL clots were prepared by mixing 75 mL of degassed bovine blood and 3 mL of calcium chloride (#21107, Sigma-Aldrich Co., St. Louis MO, USA) for a final concentration of 20 mM/L. The 78 mL blood/$CaCl_2$ mixture was poured into a latex condom and tied off to form a ~5 cm diameter spheroidal volume. Once sealed, the condoms were placed into a water bath kept at 38.6 °C for 6 hours to solidify. Solidified clots were transferred to a refrigerator at 4 °C for 12 hours prior to treatment. Before treatment, clots were allowed to warm to room temperature (i.e., 23 °C).

## Aberration Correction

Aberration correction was performed to recover the pressure lost due to the temporal defocusing through each skullcap. There was less concern in correcting the attenuation induced amplitude variation across the skullcap as lesion formation with intrinsic threshold

histotripsy relies primarily on the focal region over which the pressure is above the intrinsic threshold. In fact, precision lesion formation through the skull using histotripsy has been shown even without any aberration correction (Sukovich et al. 2016). The purpose of performing aberration correction here was primarily to increase the pressure overhead for treatment with electronic focal steering. The skullcaps were fixed concentrically within the array and aligned so that the anterior and posterior, and left and right edges were equidistant from the interior of the array. The skullcaps were positioned into the array such that the geometric origin of the array was 10 mm into the skullcap relative to the cut-plane of the skullcap. A PVDF capsule hydrophone was positioned at the geometric origin of the array. The 256 array elements were triggered sequentially and the respective waveforms delivered through the skullcap were measured by the hydrophone. Using the difference in the arrival time of the peak-negative pressure for each element waveform, the delays required to realign the arrival of the peak-negative pressure for all 256 element waveforms were calculated and uploaded to the FPGA boards. The delay measurement performed at the single point was applied as a constant temporal offset for all phased steering locations within the treatment volume. These single location aberration correction delays were used for all electronic steering locations because a similar approach is intended to be used in future *in-vivo* and clinical treatment.

## Focal Characterization through the Skullcaps

Following aberration correction, the ultrasound field produced at each frequency through each skullcap was characterized. This was done by obtaining the one-dimensional (1D) pressure profile along the 3 axes of the skullcaps and measuring pressure as a function of electronic focal steering through each skullcap.

**Beam Profiles—**To characterize the extent of focusing through each skullcap at 250 and 500 kHz, 1D beam profiles around the geometric focus were obtained with the skullcap positioned in the array. Beam profiles were measured at low pressure (i.e., < 2 MPa) using a PVDF capsule hydrophone. The hydrophone was positioned to the focus and scanned ± 25 mm from the geometric origin in 0.25 mm steps along the sagittal, coronal and axial axes. As intrinsic threshold histotripsy is dependent on the peak-negative pressure, beam profiles were constructed in reference to the peak-negative pressure at each hydrophone position. For each skull and frequency, the −6 dB beam width along each axis was measured.

**Pressure vs. Electronic Focal Steering—**To understand electronic focal steering through each skullcap at each frequency, the focal pressure as a function of electronic focal steering location was measured across a ± 20 mm range of locations centered at the geometric origin. The array was steered in 1 mm steps in the sagittal, coronal and axial dimension. For each steering location a PVDF capsule hydrophone was positioned to the location and used to measure the peak-negative pressure. To ensure the hydrophone was not damaged, the array was run at a low pressure amplitude for these measurements (i.e., < 2 MPa).

**Lesion Generation with Electronic Focal Steering—**To show the ability of histotripsy to precisely generate lesions through the skullcap, a 9 × 9 grid of lesions was

generated transcranially in an RBC phantom. The RBC-agarose gel layer of the phantom was positioned in plane with the sagittal-coronal plane of the array. The grid was designed such that greatest steering distance was ± 10 mm from the geometric origin and individual focal points were separated by 2.5 mm steps in both the sagittal and coronal direction. Using the 500 kHz array and electronic focal steering, 81 steering locations were targeted. Lesions were generated by applying 200 histotripsy pulses to each focal point at an extrapolated peak-negative pressure of 36 MPa as measured through the skullcap at the geometric origin of the array. Pulses were applied at a pulse repetition frequency (PRF) of 0.5 Hz. After generating lesions within the RBC phantom, the phantom was placed on a light table and imaged with a DSLR camera (Canon, Tokyo, Japan).

### Histotripsy Treatment

To evaluate histotripsy for clot liquefaction through the skullcap, clots were mounted within the skullcap and the center of the clot volume was aligned with the geometric origin of the array (Fig. 1). This positioning of the clot within the skullcap aligned with the findings that the majority of ICH cases occur in the central region of the brain (Aguilar and Brott 2011; Zimmerman et al. 2006). Using electronic focal steering, the focus of the array was steered through a 4 cm diameter spherical volume. The volume was filled with individual focal points according to a standard hexagonal-closed-packed (HCP) lattice pattern. Although low in f-number, the focus of these transducer arrays was not spherical. Instead it was cigar shaped, with a longer axial dimension than transverse dimensions, although generated based on spherical foci, the HCP lattice pattern provided the most efficient focal point packing for volume treatment using histotripsy. This produced to a treatment volume of 33.5 mL, which corresponded well with the average clot volume for various clinical ICH studies and marked a volumetric tipping at which patient outcomes begin to correspond to a 50% or greater probability of death within 30 days of diagnosis (Zuccarello et al. 1999, Brott et al. 1997, Broderick et al. 1993). For each frequency, the lattice focal point spacing was set to different fractions of a wavelength, specifically: $\lambda/2$, $2\lambda/3$ and $\lambda$. The focal spacing and the total number of treatment points for each case are shown in Table 2. Each treatment was applied at an overall pulse repetition frequency (PRF) of 200 Hz with 50 histotripsy pulses applied to each treatment location, corresponding to a duty cycle of 0.08% for 250kHz and 0.04% for 500kHz. To ensure intrinsic threshold histotripsy the pulse length was kept short (≤ 2 acoustic cycles or ≤ 4μs at 500 kHz and ≤ 8 μs at 250 kHz). The intrinsic threshold within the clots was expected to be consistent between frequencies (i.e., about 27 MPa) (Vlaisavljevich et al. 2015a). The number of pulses per point was chosen to minimize the number of total pulses while providing effective lesion generation. Based on previous studies, using 50 pulses per point provides well-defined lesion formation at pressures in excess of the intrinsic threshold (Lin et al. 2014). In choosing the PRF, we wanted to choose the fastest overall repetition rate that kept the PRF for a single location less than 1 Hz to avoid the cavitation memory effect described previously (Wang et al. 2012). Since the minimum number of points to fill the treatment volume across parameter combinations was 217 points, an overall PRF of 200 Hz satisfied this requirement. Linear extrapolated peak-negative pressures applied through the skullcaps of 35 and 70 MPa were used for the 250 and 500 kHz array, respectively. These different pressures were used to achieve approximately equivalent pressures at the periphery of the treatment region (i.e., furthest

steering location from the geometric focus) at the two different frequencies. The peak-negative pressure at the periphery of the treatment region was in the range of 50–83% and 20–64% of the focal peak-negative pressure (i.e., geometric focus) for the 250 and 500 kHz treatment, respectively. The total clot volume liquefied with histotripsy was measured posttreatment by inserting the catheter into the clot and drawing off the liquefied volume using a 10 mL syringe. To ensure the reported drainage volumes corresponded to that resulting from histotripsy treatment only, 12 control clots, unexposed to histotripsy were drained using the same technique (control volume). The effective clot volume liquefied by histotripsy (liquefaction volume) with each frequency and focal spacing combination was calculated as the volume aspirated via the catheter minus the control volume. For each frequency and focal spacing combination, 6 clots were treated.

### Gross Morphology and MRI

The gross morphology of blood clots was analyzed pre and post treatment by cutting a control, treated undrained and treated drained clot in half. The clots were imaged using a DSLR camera. T2-weighted MR images of the clots pre and post treatment were also obtained using a 7T MRI scanner (Varian, Inc., Palo Alto, CA, USA). The clot images were captured using a fast spin-echo (FSE) sequence.

### Skullcap Temperature Monitoring

To measure the temperature-rise of each skullcap during histotripsy treatment, four thermocouples (K-094, Physitemp Instruments Inc, Clifton, NJ, USA) were embedded directly into bone via holes slightly smaller than the thermocouple diameter such that bone made direct contact with the thermocouples. Thermocouples were positioned throughout each skullcap such that the locations were of varying thickness and gave a reasonable temperature distribution across each skullcap. Thermocouples were not positioned at the most superior portion of the skullcap as there were no elements within the central region of the array scaffold. Using the 500 kHz array, histotripsy was applied at an equivalent pressure and PRF as that used during the clot treatment experiments (i.e., 70 MPa and 200 Hz). Prior to treatment the skullcaps and surrounding water were at room temperature (23 °C). The temperature of the skullcap at each thermocouple location was measured and recorded for a total of 60 minutes. For each skullcap, histotripsy treatment was initiated approximately one minute after temperature monitoring started. Only the 500 kHz array and a 60-minute timespan were used as this was expected to show the most significant skull heating induced by histotripsy for the experiments in this paper. To approximate whether the temperature rise in the skullcaps was something capable of causing thermal damage to the skull and surrounding tissues, the average cumulative equivalent minutes at 43 °C ($CEM_{43}$) for each skullcap was calculated and compared with those $CEM_{43}$ values reported to cause tissue damage. Since temperature monitoring was performed at room temperature (~ 20 °C) and not body temperature, the $CEM_{43}$ values were calculated by adding a constant 37 °C offset to the average temperature change through each skullcap and using the equation provided in (Yarmolenko et al. 2011).

### Post Hoc B-mode Analysis of External Skull Surface During Treatment

To examine how histotripsy affected the external surface of a bleached skullcap during treatment with both the 250 and 500 kHz array, b-mode imaging of the surface of a bleached skull during treatment was performed following the initial set of experiments. A linear ultrasound probe (L-14, Ultrasonix, BK Ultrasound, Peabody, MA, USA) was inserted coaxially through the opening in the back of each array such that it was outside the sound field but sufficiently close to image the external surface of the skull. B-mode images were captured with the array off and on. This was done for both the 250 and 500 kHz array.

### Statistical Analysis

In order to understand the relationship between the histotripsy clot liquefaction results obtained from the different treatment parameters and skullcaps used in this study, statistical analysis was performed. Three sets of independent, two-tailed, two-sample Student's t-tests ($\alpha = 0.05$) were performed on the two main sets of data: volume drained due to histotripsy and the histotripsy clot liquefaction rate. The first set of t-tests analyzed the variation in results obtained between different focal spacing, holding the skullcap and frequency constant. The second set analyzed results obtained between different skullcaps holding focal spacing and frequency constant. The third set of t-tests analyzed the variation in results between different frequencies holding focal spacing and skullcap constant. By performing this set of multiple t-tests, we were able to analyze the volume liquefaction and rate effects of focal spacing for a given frequency, frequency for a given focal spacing and the variation across different skullcaps. Although comparisons between other parameter combinations was possible, the preceding analysis exhausted those comparisons pertaining to the design of the study. Any other comparisons made were post-hoc and performed after looking at the data. All comparisons made throughout this paper were considered statistically significant for p-value $< 0.05$.

## Results

### Focal Characterization through the Skullcaps

**Beam Profiles—**To characterize the extent of focusing through each skullcap using the 250 and 500 kHz arrays, 3-axis 1D beam profiles around the geometric focus were obtained with the skullcaps positioned in the array. Figure 2 shows the beam profiles at 250 and 500 kHz through skull 1. For a given frequency, the general shape of the profile was consistent through each skullcap. Along each axis, profiles at 250 kHz were more spatially spread than those at 500 kHz. The −6-dB beam widths along each axis for each skullcap and frequency are shown in Table 2.

**Pressure vs. Electronic Focal Steering—**To understand electronic focal steering through each skullcap with the 250 and 500 kHz array, the focal pressure as a function of electronic focal steering location was measured. Figure 3 shows the normalized peak-negative pressure as a function of electronic steering location for each skullcap at each frequency. For a given frequency the steering pressure profiles were similar for each skullcap. Along each axis, the pressure for the 500 kHz frequency decreased more rapidly than at 250 kHz, with the greatest differences in pressure occurring at the furthest steering

locations from the geometric focus (i.e., ± 20 mm). The percentages for the average pressure decrease, across the three skullcaps, at −20 and +20 mm for each axis relative to the geometric focal pressure are show in Table 3. In general, at 500 kHz, the pressure decrease at the steering locations furthest from the geometric focus was approximately double that at 250 kHz.

**Lesion Generation with Electronic Focal Steering—**To show the ability of histotripsy to precisely generate lesions through the skullcap with electronic focal steering, lesions were generated transcranially in an RBC phantom at a range of steering locations. Figure 4 shows a 9 × 9 grid of lesions generated through a skullcap using electronic focal steering with the 500 kHz array. The distance between the center of each lesion was approximately 2.5 mm, which matched that specified with the applied electronic focal steering. Larger and distinct lesions were generated closer to the geometric origin while smaller, indistinct lesions were generated toward the corners of the grid beyond 10 mm from the geometric focus.

## Histotripsy Treatment

For each frequency, the focus of the array was steered through a 4 cm diameter sphere corresponding to 33.5 mL. The gross morphology and MRI (Fig. 5 and 6) of a clot treated through a skullcap at 500 kHz with λ/2 focal spacing show the region of the clot liquefied with histotripsy. For each parameter combination, a total of 6 clots was treated through each skullcap. The liquefaction volume was reported as the average volume drained from treatment clots after subtracting the average volume drained from 12 control clots. In all experiments, effective clot liquefaction was achieved and drained with a catheter, in range of 6 – 59 mL in 0.9 – 42.4 minutes. The average liquefaction volume and rate with standard deviation for each combination of treatment parameters are shown in Figure 7 and Figure 8, respectively. The fastest liquefaction rate was 16.6 mL/min (15 mL in 0.9 min). The average control volume subtracted from the liquefaction volume of treated clots was 2.9 ± 1.8 mL (n = 12). The p-values for the multiple t-tests performed between the parameter combinations are shown in Tables 4 and 5.

## Effects of Frequency

Across all skullcaps and focal spacing combinations, treatment with the 500 kHz array resulted in greater liquefaction volumes than the 250 kHz array. For example, after treatment through skull 2 at λ spacing, the average liquefaction volume was 37.1 ± 16.9 mL for 500 kHz and 8.5 ± 2.9 mL for 250 kHz. In contrast to the liquefaction volume, the 250 kHz array produced greater liquefaction rates than the 500 kHz array across all skullcap and focal spacing combinations. For example, treatment through skull 1 at λ/2 spacing had a liquefaction rate of 2.9 ± 0.4 mL/min for 250 kHz and 0.6 ± 0.1 mL/min for 500 kHz.

During the 250 kHz treatment, small white particulate was observed to fall off the back of the skullcaps during treatment. This was not observed during 500 kHz treatments. As skullcaps were stored in a bleach-water solution to prevent algae from growing and gassing up the skullcaps, the exterior surface of the skull eventually turned white and chalky from the bleach. During the 250 kHz treatments, this white particulate fell off the back of the

skull, most likely because pre-focal cavitation eroded away the white, chalky layer caused by the bleach. Approximately halfway through treatments through skull 1, this effect seemed stopped. Analysis of the skull after treatment indicated that the white-chalky layer had been almost entirely removed with the true skull surface exposed. Skulls 1 – 3 after treatment with the 250 kHz array can be seen in Figure 9.

### Effects of Focal Spacing

Three different focal spacing values, λ/2, 2λ/3 and λ, were used to apply identical treatment sets for a given frequency and skullcap. For the 250 kHz array, the liquefaction volume decreased as the focal spacing increased. In contrast, in all cases but one (2λ/3 vs. λ through skull 1), the liquefaction rate increased as the focal spacing increased. For treatment at 500 kHz through a given skullcap, focal spacing had no effect on the liquefaction volume aside from treatment through skull 3, where the λ focal spacing treatment drained significantly less volume than the λ/2 and 2λ/3 through the same skull. In contrast, the liquefaction rate increased with focal point spacing in all cases.

### Variation across Skulls

**250 kHz Array—**For a given focal spacing, the 250 kHz array produced low variation in results across the three skullcaps. The only significant difference occurred in skull 2 at the λ/2 spacing. The volume liquefaction range for the 250 kHz array was 6 to 33 mL. The minimum liquefaction volume occurred through skull 3 with the λ focal spacing. The maximum occurred through skull 1 with the λ/2 focal spacing. The liquefaction rate range was 2.5 to 16.6 mL/min. The minimum rate occurred through skull 3 at a focal spacing of λ/2. The maximum occurred through skull 2 at a focal spacing of λ.

**500 kHz Array—**There was a greater variation in results across the three skullcaps for the 500 kHz treatment. Treatment through skull 1 with the 500 kHz array drained less volume for the λ/2 and 2λ/3 than the same treatments through skull 2 or 3. The volume liquefaction range for the 500 kHz array was 18 to 59 mL. Both the minimum and maximum liquefaction volume occurred through skull 2 with λ focal spacing. The liquefaction rate range was 0.6 to 8.1 mL/min. The minimum liquefaction rate occurred through skull 1 at the λ/2 focal spacing. The maximum occurred through skull 2 at the λ focal point spacing.

### Skull Temperature Monitoring

Each skullcap showed a similar trend with respect to the temperature-rise over time (Fig. 10). That is, within the first 10 minutes, there was a steep increase in temperature followed by a more gradual increase in temperature for the remainder of the time. This gradual temperature increase is likely attributed to a gradual increase in temperature in the surrounding water, which was not accounted for. For each skullcap, the maximum temperature rise remained less than 4 °C. The temperature rise measured by different probes in the skullcaps showed a variation in temperature based on the location of the probe. For skullcaps 1 – 3, the probe measurements varied between 1.9 and 3.5, 2.5 and 3.6 and 2.1 and 2.8 °C, respectively. Average values for the $CEM_{43}$ for skullcaps 1 – 3 calculated according to (Yarmolenko et al. 2011) were 0.32 ± 0.11, 0.66 ± 0.19 and 0.22 ± 0.08 minutes, respectively. These were roughly two orders of magnitude less than those thermal dose

thresholds reported to cause damage to bone and bone marrow ($CEM_{43}$ > 16 minutes) (Yarmolenko et al. 2011).

### Post Hoc B-mode Imaging of External Skull Surface During Treatment

To examine how histotripsy affected the external surface of a bleach skullcap during treatment, B-mode imaging of the surface of a bleached skull was performed following the initial set of experiments. Figure 11 shows the B-mode images of the external skull surface with the array off, on at 250 kHz and on at 500 kHz. There was a noticeable cloud of particulate that formed with the 250 kHz array on that was not present with the array off. This was not observed with the 500 kHz array.

## Discussion

The results demonstrate the use of histotripsy with electronic focal steering for fast transcranial clot liquefaction. Using electronic focal steering, it was possible to generate precise lesions through the excised human skullcaps and ultimately liquefy a 4 cm spherical volume within clots. By examining combinations of frequency and focal point spacing for electronically steered transcranial histotripsy treatment, volumes as large as 59 mL were liquefied within maximum treatment times (42.4 minutes) well below those of other minimally invasive techniques used to treat ICH. The concerns of skull heating associated with histotripsy were minimal with the average $CEM_{43}$ values through three different skullcaps approximately two orders of magnitude lower than those reported to cause damage to bone and bone marrow.

As the success of transcranial histotripsy ICH treatment is dependent upon removing the majority of the region of clot insonated in the minimum amount of time, the optimal parameter combination consists of a balance between the liquefaction volume and rate. Overall, the 250 kHz treatments produced much faster liquefaction rates than those at 500 kHz. However, the volumes drained at these large liquefaction rates produced with the 250 kHz array were much lower than those produced with the 500 kHz array (e.g., for skull 3, 250 kHz with $\lambda$ spacing produced 6.63 mL while that at 500 kHz produced 25.38 mL). Based on the results shown here, the optimal treatment parameter combination among the ones tested was either the $\lambda$ focal spacing applied at 500 kHz or the $\lambda/2$ focal spacing applied at 250 kHz. A post-hoc two-tailed t-test ($\alpha = 0.05$) showed no difference between the two parameter combinations with both producing large volume liquefaction at fast rates. However, the erosion of the external surface of the skullcap observed at 250 kHz was a significant concern. As this was not observed at 500 kHz, the $\lambda$ focal spacing applied at 500 kHz is suggested as the optimal treatment parameter combination among the ones tested, as it was able to produce sufficiently large liquefaction volumes through skullcaps 1 – 3 (23.1 ± 4.0, 37.1 ± 16.9 and 25.4 ± 3.2 mL) with fast liquefaction rates (3.2 ± 0.6, 5.1 ± 2.3 and 3.5 ± 0.4 mL/min). Based on the bovine clot model used in this study, this presents an 11 – 33-fold increase in treatment rate when compared with current studies using MRgFUS, the fastest of the current minimally invasive ICH treatments under investigation (Monteith et al. 2013a; Monteith et al. 2013b; Monteith et al. 2013c; Ramanan and Shankar 2013). However, it should be noted that our clot model differed slightly from those used in the

aforementioned MRgFUS studies which used either fresh porcine or human blood clotted at room temperature and could present discrepancies in the reported improvement. In regards to the current clinical minimally invasive treatments with rt-PA, the liquefaction volumes reported here are of a similar order as those shown in the literature (Morgan et. al. 2008). However, the treatment time with rt-PA remains orders of magnitude greater than the treatment times reported in this study.

Overall, liquefaction volumes produced at 500 kHz were larger across all skullcap and focal point spacing combinations relative to those produced at 250 kHz. In addition, the 500 kHz liquefaction volumes were largely independent of focal spacing, something that was not observed at 250 kHz. An understanding of the reasons for this can be approached by considering the pressure steering profiles and the geometric focal pressure for the 250 and 500 kHz array. As the lesion size correlates well with the dimensions of the focus above the intrinsic threshold (Vlaisavljevich et al. 2017) and the 1D beam profiles (Fig. 2) show a much larger focal region at 250 kHz, the focal spacing was made proportional to the frequency of the array. This doubled the size of the absolute focal spacing at 250 kHz compared to that at 500 kHz. With identical peak-negative pressures across the entire treatment region, we would expect similar liquefaction results between the two frequencies for each focal spacing. However, due to the difference in the pressure steering profiles between the two frequencies (Fig. 3), there was an inherent challenge in comparing treatment between two different frequencies with electronic focal steering. To sustain either uniform pressure profiles or equivalent pressure profiles between frequencies, the pressure output from the array would need to be modulated across a large range quickly enough to keep up with the PRF of the applied treatment. Although this is a possibility with the current driving system, this technique of sustaining consistent pressures across an electronic focal steering volume has not yet been thoroughly investigated. However, by keeping pressures at the largest steering radii (± 20 mm from the geometric focus) approximately equal between the two frequencies (Table 3), we ensured some degree of comparability between the treatments. Nonetheless, the higher focal gain in the 500 kHz treatments resulted in a larger peak-negative pressures applied to regions close to the geometric focus than those for the 250 kHz treatments. The effects of these field property differences between the two frequencies were likely manifested in the differences observed between liquefaction volume for a given focal spacing at each frequency.

One effect that was observed during the 250 kHz and not during 500 kHz treatment was the small amount of micron-sized particulate falling off the back of the skullcaps. Literature shows that the primary component of household bleach, sodium hypochlorite, can deproteinize the surface layer of cortical bone without disrupting the mineral composition (Boyde and Hobdell 1969; Broz et al. 1997; Kerbl et al. 2012; Otter et al. 1988). As skullcaps were stored in a bleach-water solution to prevent algae from growing prior to treatment with the 250 kHz array but not the 500 kHz array, the initial thought was that this particulate formation during the 250 kHz experiments was primarily due to the bleach-induced fragile, chalky mineral layer on the external surface of the skull that precipitated off during histotripsy treatment. However, post hoc B-mode imaging of the external surface of a bleached skullcap treated with 250 kHz and 500 kHz, showed particulate formation at 250 kHz but not 500 kHz. Therefore, the erosion of the skull surface was particular to treatment

with the 250 kHz array. Based on the B-mode images alone, it is difficult to point directly to prefocal cavitation as the cause. However, this is likely the only mechanism that would cause such an effect. If prefocal cavitation, it is possible that this occurred due to the larger beam size at 250 kHz than at 500 kHz and an increased chance of the beam interfering with the skullcap. However, the portion of the beam interfering with the skull was likely well below the intrinsic threshold and preliminary studies show the 500 kHz focus can be positioned close (within 5 mm) to the skullcap without causing the effects seen here at 250 kHz, suggesting that something else is causing the prefocal cavitation at 250 kHz. One thought is that the likelihood of prefocal cavitation increases at lower frequency, which is based on the observation that the probability of producing "incidental cavitation bubbles" (occurring at pressures below intrinsic threshold) is greater at lower frequencies than at higher frequencies (Vlaisavljevich et al. 2015a). The increased likelihood of initiating incidental bubbles in combination with a high PRF to sustain the "incidental bubbles" might have resulted in the presence of prefocal cavitation at 250 kHz and not at 500 kHz. Future cavitation detection experiments with time windowing at the skull surface should be able to validate prefocal cavitation as the cause.

The concern for histotripsy induced skull heating was minimal in that the average $CEM_{43}$ values for each skullcap were about two orders of magnitude lower than those reported to cause damage in bone and bone marrow (Yarmolenko et al. 2011). Due to the in-vitro nature of these experiments, the heat sink effects into skin and brain tissue were not examined in this study and remain a concern requiring further analysis. However, based on the $CEM_{43}$ values reported to cause damage in skin and brain tissue, these initial skull heating results are promising. Skin damage has not been reported for $CEM_{43}$ values less than 20 minutes. Although the $CEM_{43}$ threshold for brain damage is lower and a bit more complicated than that of skin and bone with a range of values depending on the region, any concerns of the skull heat sink effects overheating brain tissue could be mitigated by reducing PRF if necessary. Skull heating has been a major issue for MRgFUS, limiting the treatment location profile and treatment rate. In certain *in-vivo* and *in-vitro* MRgFUS studies, to reduce the heating, cool water was continuously circulated over the skull (McDannold et al. 2010; Hynynen et al. 2006b). The clot liquefaction and skull heating results presented in this study show the ability of histotripsy to perform rapid clot liquefaction while suggesting the potential of keeping the skull and surrounding tissue within a safe temperature range. However, although these experiments provided a good starting point to analyze the potential of unwanted heating effects caused by histotripsy, it is difficult to claim how they will translate to in-vivo or clinical cases where surrounding tissues and perfusion may contribute to histotripsy induced temperature changes.

As the majority of ICH cases occur in the central region of the brain (Aguilar and Brott 2011; Zimmerman et al. 2006). The central position of the clots within the skullcaps in this study was a reasonable starting point for analyzing the potential of histotripsy to liquefy clots representative of ICH. However, the remaining ICH cases occur in off center brain regions such as the cortical lobes, cerebellum and brainstem. In this study, we chose to limit our investigation to the liquefaction of a clot volume located in what would be the central region of the brain and the potential to treat volumes off-center was not examined. By mechanically repositioning the skull or the array, these regions can be reached. However,

this mechanical repositioning may cause changes to skull heating and thus requires further investigation.

The results throughout this paper have been reported as “liquefaction volumes” drained from treated clots with a catheter and 10 mL syringe. This drainage technique was used as it is expected that a similar technique will be used to remove the volume of clot liquefied with histotripsy in a clinical setting and one we are currently working to integrate with a miniature acoustic hydrophone to enable aberration correction. Histotripsy treatments targeting other organs have often attempted to completely liquefy the entire treatment region into an acellular homogenate (e.g., tumor ablation). However, in the context of ICH treatment and this study, complete liquefaction of the clot is not necessary and liquefaction needs only to be performed to the extent where the treated volume can be drained from the clot using the catheter and syringe. This can be observed in the gross morphology of the treated clot (Fig. 7), where the broken down slurry remains after treatment and is removed after drainage with the catheter. This is likely the reason it was possible to generate consistent liquefaction volumes across different focal spacing at 500 kHz. Therefore, to optimize histotripsy for ICH treatment, the goal should be to fractionate the clot sufficiently to drain from the catheter for clot removal, and small clot pieces remaining may be acceptable as long as they are small enough to drain via catheter.

## Conclusion

This study investigated the effects of ultrasound frequency and focal spacing on the treatment efficacy and treatment speed alongside the temperature rise in the skull during transcranial histotripsy clot liquefaction. The specific emphasis of the study was to analyze the effects of transducer frequency and focal spacing on treatment efficacy and speed and show histotripsy’s feasibility for rapid, minimally invasive ICH treatment. The fastest liquefaction rate across all clot treatments was 16.6 mL/min (15 mL in 0.9 min). The λ focal spacing applied at 500 kHz is suggested as the best treatment parameter combination among those tested, as it was able to produce large liquefaction volumes through skullcaps 1 – 3 (23.1 ± 4.0, 37.1 ± 16.9 and 25.4 ± 16.9 mL) with the fast liquefaction rates (3.2 ± 0.6, 5.1 ± 2.3 and 3.5 ± 0.4 mL/min), presenting an 11 – 33-fold increase in treatment rate when compared with treatments using MRgFUS and orders of magnitude faster than clinical minimally invasive techniques using rt-PA. In addition, the skull heating effects of transcranial histotripsy at the parameter combinations examined in this study indicated minimal concern with average $CEM_{43}$ values about two orders of magnitude lower than those reported to cause thermal damage in bone and bone marrow. Future work will focus on applying the results of this study to *in-vivo* clot treatment in a porcine model.

## Acknowledgments

This work was supported by grants from the National Institute of Neurological Disorders and Stroke (NINDS) of the National Institutes of Health (NIH) under Award Number R21-NS093121, the National Institute of Biomedical Imaging and Bioengineering (NIBIB) of the NIH under Award Number R01-EB008998 and the National Science Foundation Graduate Research Fellowship Program under Grant No. 2017239378. Disclosure notice: Drs. Charles A. Cain, Timothy L. Hall, and Zhen Xu have financial interests and/or other relationship with HistoSonics Inc.

## References


Aguilar MI, Brott TG. Update in intracerebral hemorrhage. Neurohospitalist. 2011; 1:148–59. [PubMed: 23983850]

Alexandrov AV, Demchuk AM, Burgin WS, Robinson DJ, Grotta JC. Ultrasound enhanced thrombolysis for acute ischemic stroke: Phase i. findings of the clotbust trial. J Neuroimaging. 2004; 14:113–17. [PubMed: 15095555]

Alexandrov AV, Mikulik R, Ribo M, Sharma VK, Lao AY, Tsivgoulis G, Sugg RM, Barreto A, Sierzenski P, Malkoff MD, Grotta JC. A pilot randomized clinical safety study of sonothrombolysis augmentation with ultrasound activated perflutren lipid microspheres for acute ischemic stroke. Stroke. 2008; 39:1464–69. [PubMed: 18356546]

Boyde A, Hobdell MH. Scanning electron microscopy of primary membrane bone. Z Zellforsh Mikrosk Anat. 1969; 99:98–108.

Brott T, Broderick J, Kothari R, Barsan W, Tomsick T, Sauerbeck L, Spilker J, Duldner J, Khoury J. Early hemorrhage growth in patients with intracerebral hemorrhage. Stroke. 1997; 28:1–5. [PubMed: 8996478]

Broderick JP, Brott TG, Duldner JE, Tomsick T, Huster G. Volume of intracerebral hemorrhage. A powerful and easy-to-use predictor for 30-day mortality. Stroke. 1993; 24:987–93. [PubMed: 8322400]

Broderick JP, Brott TG, Tomsick T, Tew J, Duldner JE, Huster G. Management of intracerebral hemorrhage in a large metropolitan population. Neurosurg. 1994; 34:882–87.

Broz JJ, Simske SJ, Corley WD, Greenberg AR. Effects of deproteinization and ashing on site-specific properties of cortical bone. 1997; 8:395–401.

Datta S, Coussios CC, McAdory LE, Tan J, Porter T, de Courten-Myers GM, Hollan CK. Correlation of cavitation with ultrasound enhancement of thrombolysis. 2006; 32:1257–67.

Datta S, Coussios CC, Ammi AY, Mast TD, de Courten-Myers, Holland CK. Ultrasound-enhanced thrombolysis using definityR as a cavitation nucleation agent. Ultrasound Med Biol. 2008; 34:1421–33. [PubMed: 18378380]

Dennis MS. Outcome after brain haemorrhage. Cerebrovasc Dis. 2003; 16:9–13. [PubMed: 12698013]

Elias WJ, Huss D, Voss T, Loomba J, Khaled M, Frysinger RC, Sperling S, Wylie S, Monteith S, Druzgal J, Shah B, Harrison M, Wintermark M. The use of magnetic resonance- guided high intensity focused ultrasound to treat essential tremor. J Acoust Soc Am. 2013; 134:4090.

Elias WJ, Huss D, Voss T, Loombda J, Khaled M, Zadicario E, Frysinger RC, Sperling S, Wylie S, Monteith S, Druzgal J, Shah B, Harrison M, Wintermark M. A pilot study of focused ultrasound thalamotomy for essential tremor. N Engl J Med. 2013; 7:640–48.

Fernandes HM, Gregson B, Siddique S, Mendelow AD. Surgery in intracerebral hemorrhage the uncertainty continues. Stroke. 2000; 31:2511–16. [PubMed: 11022087]

Flaherty ML, Haverbusch M, Sekar P, Kissela B, Kleindorfer D, Moomaw CJ, Sauerebeck L, Schneider A, Broderick JP, Woo D. Long-term mortality after intracerebral hemorrhage. Neurology. 2006; 66:1182–86. [PubMed: 16636234]

Go AS, Mozaffarian D, Roger VL, Benjamin EJ, Berry JD, Borden WB, Bravata DM, Dai S, Ford ES, Fox CS, Franco S, Fullerton HJ, Gillespie C, Hailpern SM, Heit JA, Howard VJ, Huffman MD, Kissela BM, Kittner SJ, Lackland DT, Lichtman JH, Lisabeth LD, Magid D, Marcus GM, Marelli A, Matchar DB, McGuire DK, Mohler ER, Moy CS, Mussolino ME, Nchol G, Paynter NP, Schreiner PJ, Sorlie PD, Stein J, Turan TN, Virani SS, Wong ND, Woo D, Turner MB. Executive summary: heart disease and stroke statistics—2013 update: a report from the American Heart Association. Circ. 2013; 127:143–52.

Hankey GJ, Hon C. Surgery for primary intracerebral hemorrhage: is it safe and effective? A systematic review of case series and randomized trials. Stroke. 1997; 28:2126–32. [PubMed: 9368552]

Hattori A, Katayama Y, Maya Y, Gaherer A. Impact of stereotactic hematoma evacuation on medical costs during the chronic period in patients with spontaneous putaminal hemorrhage: a randomized study. Surg Neurol. 2006; 65:429–35. [PubMed: 16630899]

Hitchcock KE, Holland CK. Ultrasound-assisted thrombolysis for stroke therapy better thrombus break-up with bubbles. Stroke. 2010; 41:S50–3. [PubMed: 20876505]

Holland CK, Vaidya SS, Datta S, Coussios CC, Shaw GJ. Ultrasound-enhanced tissue plasminogen activator thrombolysis in an in vitro porcine clot model. 2008; 121:663–73.

Hynynen K, McDannold N, Vykhodtseva N, Raymond S, Weissleder R, Jolesz FA, Sheikov N. Focal disruption of the blood-brain barrier due to 260-kHz ultrasound bursts: a method for molecular imaging and targeted drug delivery. J Neurosurg. 2006; 105:445–54. [PubMed: 16961141]

Hynynen K, McDannold N, Clement G, Jolesz FA, Zadicario D, Killiany R, Moore T, Rosen D. Pre-clinical testing of a phased array ultrasound system for MRI-guided noninvasive surgery of the brain-a primate study. Eur J Radiol. 2006; 59:149–56. [PubMed: 16716552]

Kerbl FM, Devilliers P, Litake M, Eleazer PD. Physical effects of sodium hypochlorite on bone: an *ex vivo* study. J Endod. 2012; 38:357–59. [PubMed: 22341074]

Khokhlova TD, Monsky WL, Haider YA, Maxwell AD, Wang Y, Matula TJ. Histotripsy liquefaction of large hematomas. Ultrasound Med Biol. 2016; 42:1491–98. [PubMed: 27126244]

Kieran K, Hall TL, Parsons JE, Wolf JS Jr, Fowlkes JB, Cain CA, Roberts WW. Refining histotripsy: Defining the parameter space for the creation of nonthermal lesions with high intensity, pulsed focused ultrasound of the in vitro kidney. J Urol. 2007; 178:672–76. [PubMed: 17574617]

Kim Y, Hall TL, Xu Z, Cain CA. Transcranial histotripsy therapy: a feasibility study. IEEE Trans Ultrason Ferroelectr Freq Control. 2014; 61:582–93.

Kim Y, Maxwell AD, Hall TL, Xu Z, Lin K, Cain CA. Rapid prototyping fabrication of focused ultrasound transducers. IEEE Trans Ultrason Ferroelectr Freq Control. 2014; 61:1559–74. [PubMed: 25167156]

Kulina EV, Tong X, George MG, Bansil P. Epidemiology and prevention of stroke: a worldwide perspective. Expert Rev Neurother. 2012; 12:199–208. [PubMed: 22288675]

Lin K-W, Kim Y, Maxwell AD, Wang T, Hall TL, Xu Z, Fowlkes JB, Cain CA. Histotripsy beyond the “intrinsic” threshold using very short ultrasound pulses: “microtripsy”. IEEE Trans Ultrason Ferroelectr Freq Control. 2014; 61:251–65. [PubMed: 24474132]

Maxwell AD, Cain CA, Duryea AP, Yuan L, Gurm HS, Xu Z. Noninvasive thrombolysis using pulsed ultrasound cavitation therapy – histotripsy. Ultrasound Med Biol. 2009; 35:1982–94. [PubMed: 19854563]

Maxwell AD, Wang T-Y, Yuan L, Duryea AP, Xu Z, Cain CA. A tissue phantom for visualization and measurement of ultrasound-induced cavitation damage. Ultrasound Med Biol. 2010; 39:449–465.

Maxwell AD, Owens G, Gurm HS, Ives K, Myers DD Jr, Xu Z. Noninvasive treatment of deep venous thrombosis using pulsed ultrasound cavitation therapy (histotripsy) in a porcine model. J Vasc Interv Radiol. 2011; 22:369–77. [PubMed: 21194969]

Maxwell AD, Cain CA, Hall TL, Fowlkes JB, Xu Z. Probability of cavitation for single ultrasound pulses applied to tissues and tissue-mimicking materials. Ultrasound Med Biol. 2013; 39:449–465. [PubMed: 23380152]

McDannold N, Park E-J, Mei C-S, Zadicario E, Jolesz F. Evaluation of three-dimensional temperature distributions produced by a low-frequency transcranial focused ultrasound system within ex vivo human skulls. IEEE Trans Ultrason Ferroelectr Freq Control. 2010; 57:1967–76. [PubMed: 20875986]

Meairs S, Alonso A, Hennerici MG. Progress in sonothrombolysis for treatment of stroke. Stroke. 2012; 43:1706–10. [PubMed: 22535275]

Mendelow AD, Gregson BA, Fernandes HM, Murray GD, Teasdale GM, Hope DT, Karimi A, Shaw MD, Barer DH. Early surgery versus initial conservative treatment in patients with spontaneous supratentorial intracerebral haematomas in the Internation Surgical Trial in Intracerebral Haemorrhage (STICH): a randomised trial. Lancet. 2005; 365:387–97. [PubMed: 15680453]

Mendelow AD, Gregson BA, Rowan EN, Murray GD, Gholkar A, Mitchell PM. Early surgery versus initial conservative treatment in patients with spontaneous supratentorial lobar intracerebral haematomas (STICH II): a randomised trial. Lancet. 2013; 382:397–408. [PubMed: 23726393]

Monteith SJ, Harnof S, Medel R, Popp B, Wintermark M, Lopes MB, Kassel NF, Elias WJ, Snell J, Eames M, Zadicario E, Moldovan K, Sheehan J. Minimally invasive treatment of intracerebral

hemorrhage with magnetic resonance-guided focused ultrasound. J Neurosurg. 2013; 118:1035–45. [PubMed: 23330996]

Monteith SJ, Kassell NF, Goren O, Harnof S. Transcranial MR-guided focused ultrasound sonothrombolysis in the treatment of intracerebral hemorrhage. Neurosurg Focus. 2013; 34:E14. [PubMed: 23634918]

Monteith SJ, Sheehan J, Medel R, Wintermark M, Eames M, Snell J, Kassell NF, Elias WJ. Potential intracranial applications of magnetic resonance-guided focused ultrasound surgery. J Neurosurg. 2013; 118:215–21. [PubMed: 23176339]

Morgan T, Zuccarello M, Narayan R, Keyl P, Lane K, Hanley D. Preliminary findings of the minimally-invasive surgery plus rtPA for intracerebral hemorrhage evacuation (MSITIE) clinical trial. Acta Neurochir Suppl. 2008; 105:147–51. [PubMed: 19066101]

Nance E, Timbie K, Miller GW, Song J, Louttit C, Klibanov AL, Shih T-Y, Swaminathan G, Tamargo RJ, Woodworth GF, Hanes J, Price RJ. Noninvasive delivery of stealth, brain-penetrating nanoparticles across the blood-brain barrier using MRI-guided focused ultrasound. J Control Release. 2014; 189:123–32. [PubMed: 24979210]

O'Reilly MA, Hynynen K. Ultrasound enhanced drug delivery to the brain and central nervous system. Int J Hyperthermia. 2012; 28:386–96. [PubMed: 22621739]

Otter M, Goheen S, Williams WS. Streaming potentials in chemically modified bone. J Orthop Res. 1988; 6:346–59. [PubMed: 2833592]

Pajek D, Hynynen K. The design of a focused ultrasound transducer array for the treatment of stroke: a simulation study. Phys Med Biol. 2012; 57:4951–68. [PubMed: 22800986]

Parsons JE, Cain CA, Fowlkes JB. Cost-effective assembly of a basic fiber-optic hydrophone for measurement of high-amplitude therapeutic ultrasound fields. J Acoust Soc Am. 2006; 119:1432–40. [PubMed: 16583887]

Qureshi AI, Mendelow AD, Hanley D. Intracerebral haemorrhage. Lancet. 2009; 373:1632–44. [PubMed: 19427958]

Ramanan M, Shankar A. Minimally invasive surgery for primary supratentorial intracerebral haemorrhage. J Clin Neurosci. 2013; 20:1650–58. [PubMed: 24161339]

Roberts WW, Hall TL, Ives K, Wolf JS Jr, Fowlkes JB, Cain CA. Pulsed cavitational ultrasound: a noninvasive technology for controlled tissue ablation (histotripsy) in the rabbit kidney. J Urol. 2006; 175:734–38. [PubMed: 16407041]

Vlaisavljevich E, Lin K-W, Maxwell A, Warnez MT, Mancia L, Singh R, Putnam AJ, Fowlkes B, Johnsen E, Cain C, Xu Z. Effects of ultrasound frequency and tissue stiffness on the histotripsy intrinsic threshold for cavitation. Ultrasound Med Biol. 2015; 41:1651–67. [PubMed: 25766571]

Vlaisavljevich E, Aydin O, Yuksel D, Lin K-W, Fowlkes B, Elsayed M, Xu Z. Effects of ultrasound frequency of nanodroplet-mediated histotripsy. Ultrasound Med Biol. 2015; 41:2135–47. [PubMed: 25959056]

Vlaisavljevich E, Gerhardson T, Hall T, Xu Z. Effects of *f*-number on the histotripsy intrinsic threshold and cavitation bubble cloud behavior. Phys Med Biol. 2017; 62:1269–90. [PubMed: 27995900]

Wang T-Y, Xu Z, Hall TL, Fowlkes JB, Cain CA. An efficient treatment strategy for histotripsy by removing cavitation memory. Ultrasound Med Biol. 2012; 38:753–66. [PubMed: 22402025]

Wang WZ, Jiang B, Liu HM, Li D, Lu CZ, Zhao YD, Sander JW. Minimally invasive craniopuncture therapy vs. conservative treatment for spontaneous intracerebral hemorrhage: results from a randomized clinical trial in China. Int J Stroke. 2009; 4:11–16. [PubMed: 19236490]

Wright C, Hynynen K, Goertz D. In vitro and in vivo high-intensity focused ultrasound thrombolysis. Invest Radiol. 2012; 47:217–25. [PubMed: 22373533]

Xu Z, Ludomirsky A, Eun LY, Hall TL, Tran BC, Folkes JB, Cain CA. Controlled ultrasound tissue erosion. IEEE Trans Ultrason Ferroelectr Freq Control. 2004; 51:726–36. [PubMed: 15244286]

Xu Z, Folkes JB, Rothman ED, Levin AM, Cain CA. Controlled ultrasound tissue erosion: the role of dynamic interaction between insonation and microbubble activity. J Acoust Soc Am. 2005; 117:424–35. [PubMed: 15704435]

Xu Z, Owens G, Gordon D, Cain CA, Ludomirsky A. Noninvasive creation of an atrial septal defect by histotripsy in a canine model. Circ. 2010; 121:742–49.

Yarmolenko PS, Moon EJ, Landon C, Manzoor A, Hochman DW, Viglianti BL, Dewhirst MW. Thresholds for thermal damage to normal tissues: an update. Int J Hyperthermia. 2011; 27:320–43. [PubMed: 21591897]

Zimmerman RD, Maldjian JA, Brun NC, Horvath B, Skolnick BE. Radiologic estimation of hematoma volume in intracerebral hemorrhage trial by CT scan. Am J Neuroradiol. 2006; 27:666–70. [PubMed: 16552014]

Zuccarello M, Brott T, Derex L, Kothari R, Sauerbeck L, Tew J, Loveren HV, Yeh H-S, Tomsick T, Pancioli A, Khoury J, Broderick J. Early surgical treatment for supratentorial intracerebral hemorrhage: a random feasibility study. Stroke. 1999; 30:1833–39. [PubMed: 10471432]

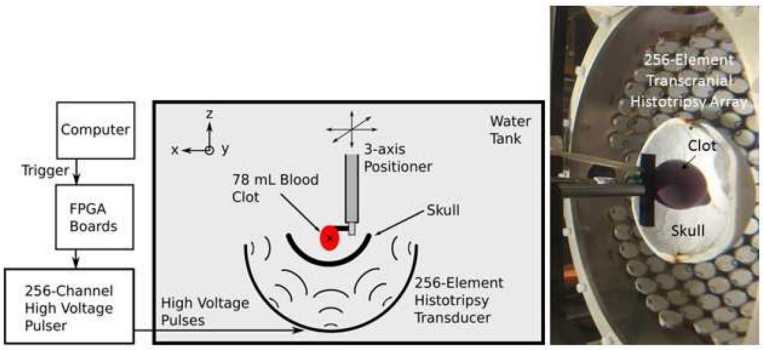


**Figure 1. Experimental Setup**

The experimental schematic of the setup used to perform the transcranial histotripsy clot treatments through the excised human skullcaps (left) and a photograph of the actual experimental setup (right). The blood clots were mounted within the skullcap and the center of the clot volume was aligned with the geometric origin of the array.

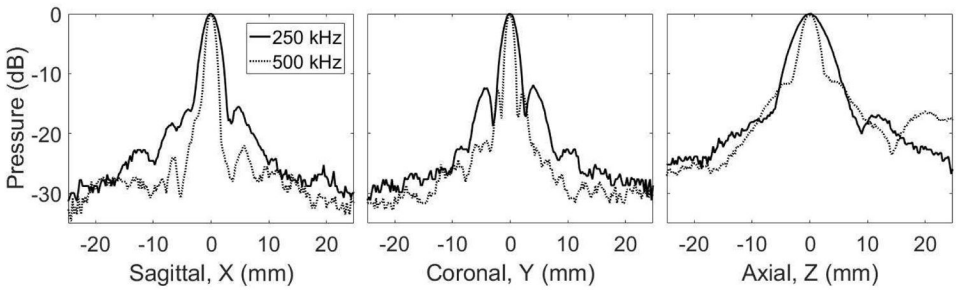


**Figure 2. 1D Beam Profiles**

The 3-axis 1D beam profiles around the geometric focus through skull 1 positioned into the array obtained at 250 and 500 kHz.

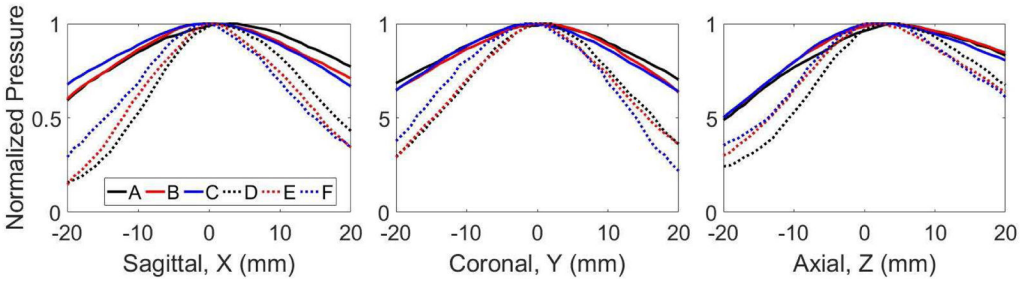


**Figure 3. Pressure vs. Electronic Focal Steering**

The peak-negative focal pressure as a function of electronic focal steering location was measured across a ± 20 mm range of locations centered at the geometric origin. Pressure steering profiles were obtained along the sagittal, coronal and axial dimension. Profile A – C correspond to the normalized pressure profile through skull 1 – 3, respectively, at 250 kHz. Profile D – F correspond to the normalized pressure through skulls 1 – 3, respectively, at 500 kHz.

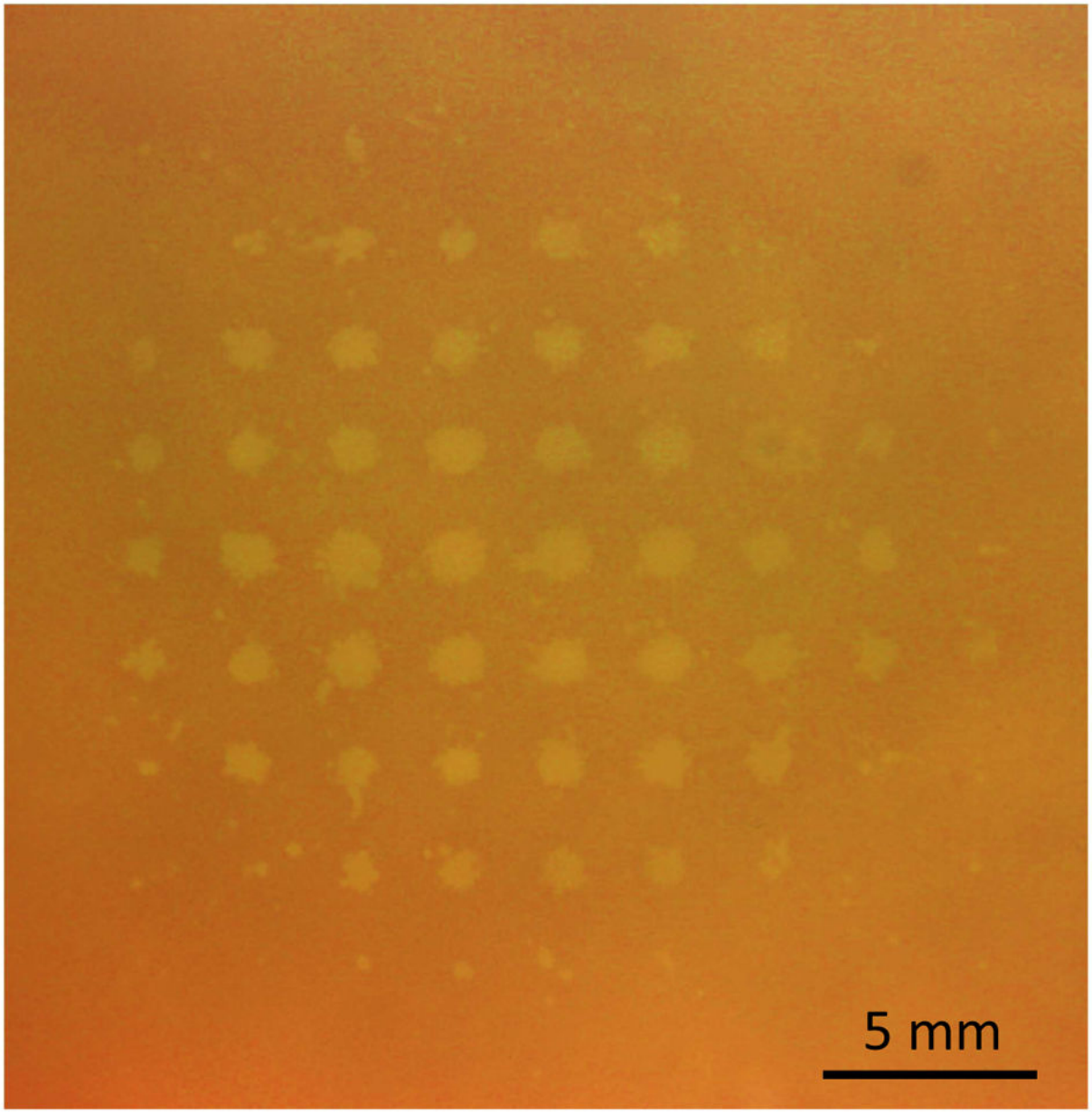


**Figure 4. Lesion Generation with Electronic Focal Steering**

A 9 × 9 grid of lesions generated through a skullcap with electronic focal steering at 500 kHz. The distance between the center of each lesion was approximately 2.5 mm, which matched the focal location spacing specified with the applied electronic focal steering.

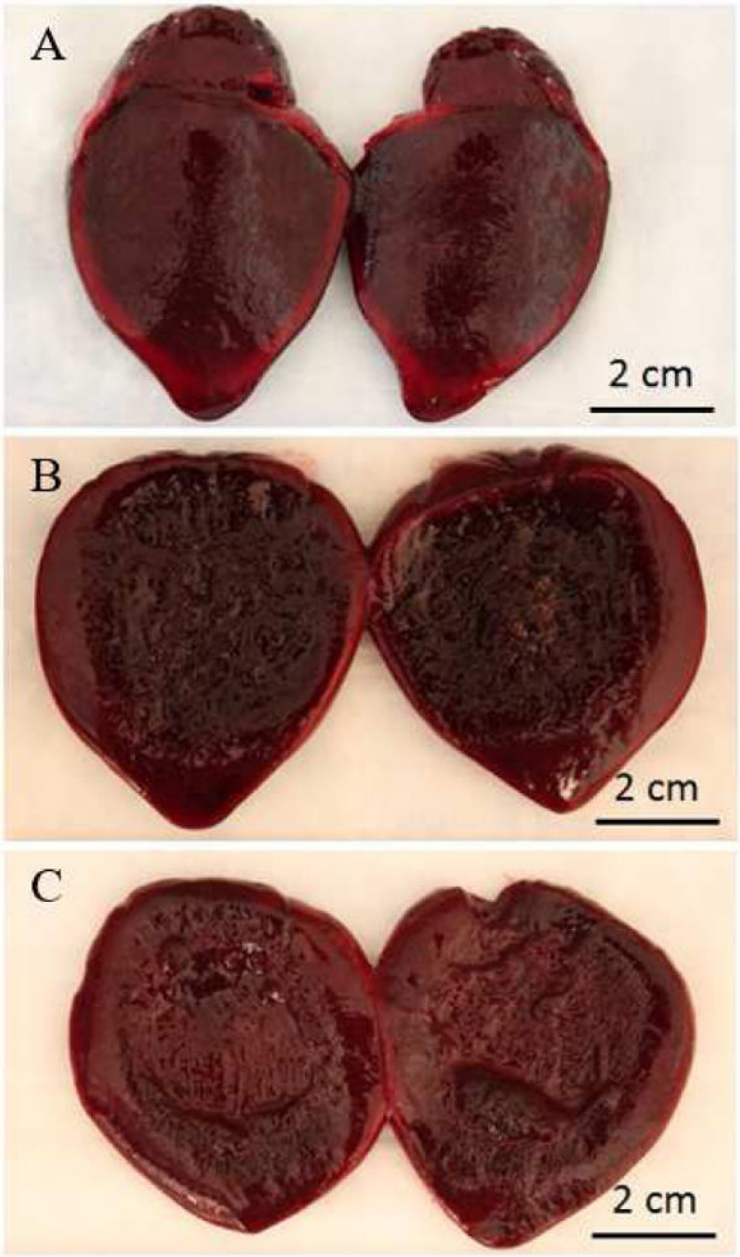


**Figure 5. Clot Gross Morphology**

The gross morphology of a (A) control clot, (B) treated, undrained clot and (C) treated, drained clot. For the treated, undrained clot, the majority of the liquefied clot spilled out after removing it from the condom and cutting it in half, leaving a broken down slurry region approximately 4 cm in diameter. The treated, drained clot showed a 4 cm diameter cavity indicating the region left after removing the broken down slurry.

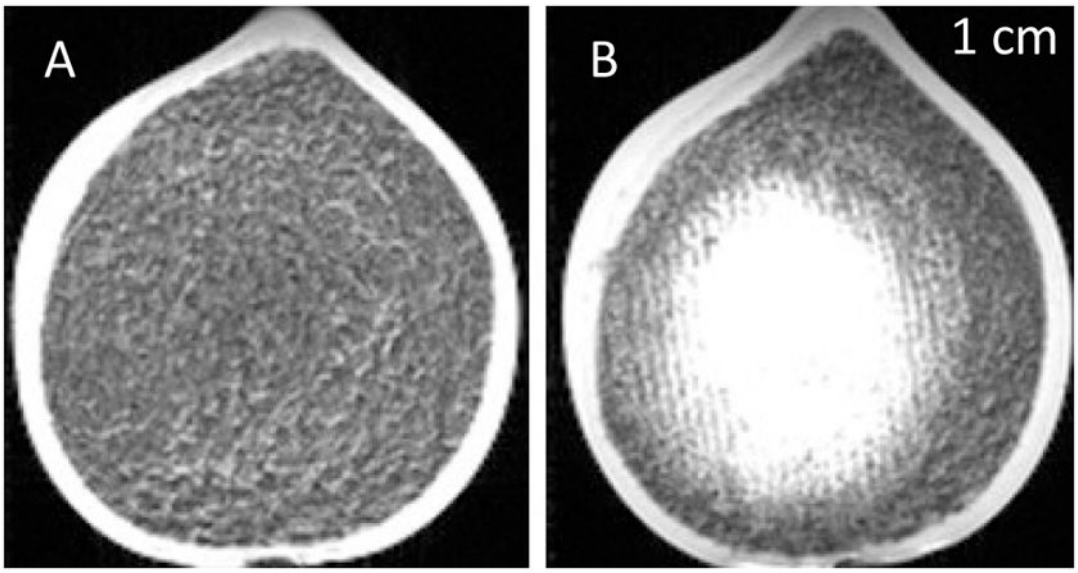


**Figure 6. Pre- and Posttreatment Clot MRI**

T2-weighted MR images of pre- and posttreatment clots for treatment with the 500 kHz array with lattice focal point spacing of λ/2. In the pretreatment images, the clot appeared uniformly dark. The posttreatment image showed a bright region approximately 4 cm in diameter that corresponded to the lysed blood cells in the liquefied clot. The bright region was densest in the center portion and became less so toward the periphery of the clot.

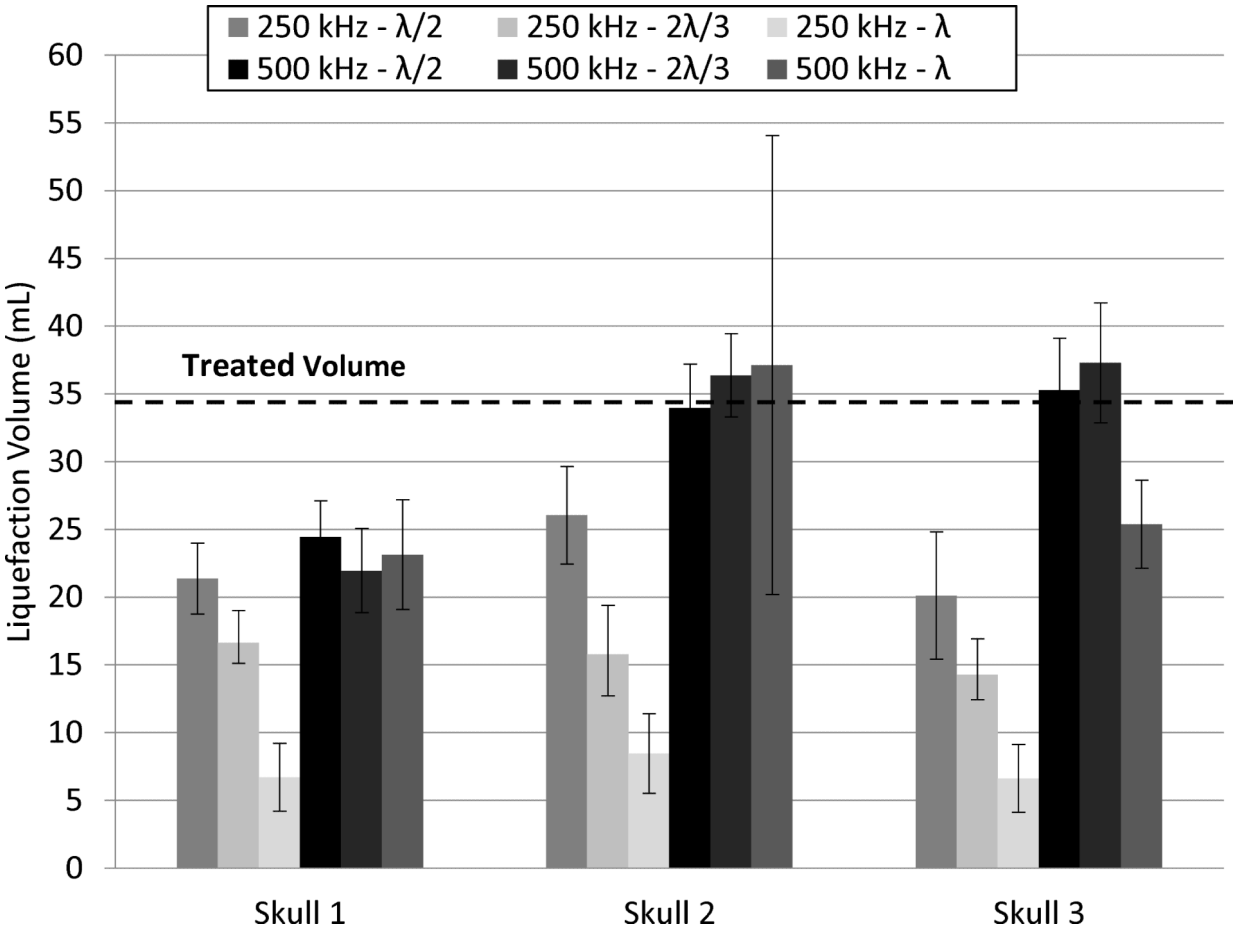


**Figure 7. Clot Liquefaction Volume**

The average clot volume liquefied with histotripsy through each skullcap (n = 6) after subtracting the average control volume (n =12). Transcranial histotripsy treatment was applied using 250 and 500 kHz arrays with lattice focal point spacing of λ/2, 2λ/3 and λ.

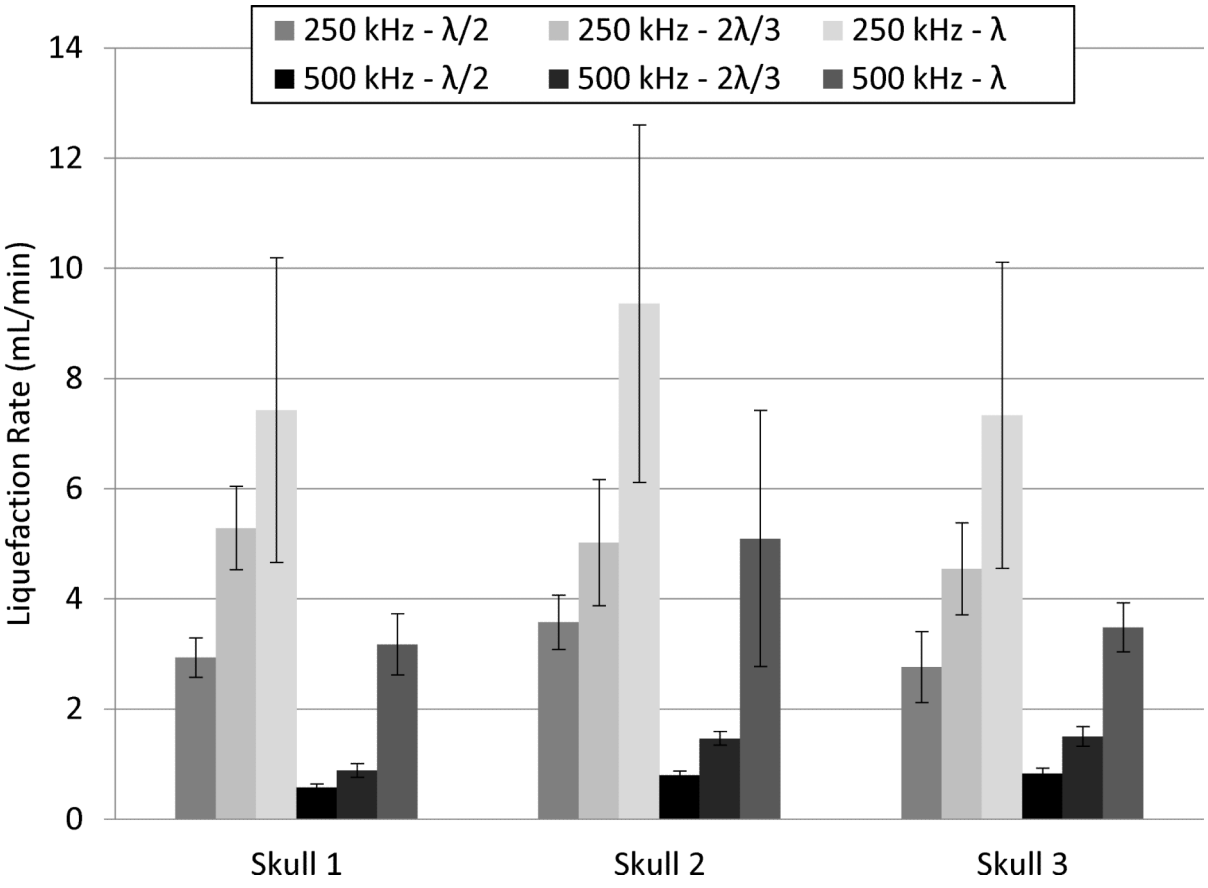


**Figure 8. Clot Liquefaction Rate**

The average liquefaction rate for each frequency and focal spacing achieved through each skullcap.

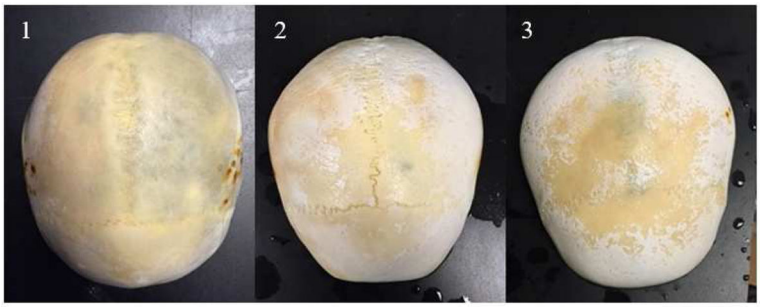


**Figure 9. Skullcaps after 250 kHz Treatment**

The external, superior portion of each skullcap after all treatments with the 250 kHz array. As skullcaps were stored in a bleach-water solution to prevent algae from growing and gassing up the skullcaps, the exterior surface of the skull eventually turned white and chalky. During the 250 kHz treatments, this white particulate fell off the back of the skull, most likely because the pre-focal cavitation eroded away the white, chalky layer caused by the bleach. Approximately halfway through treatments through skull 1, this effect stopped. Analysis of the skull after treatment indicated that the white-chalky layer had been almost entirely removed with the true skull surface exposed.

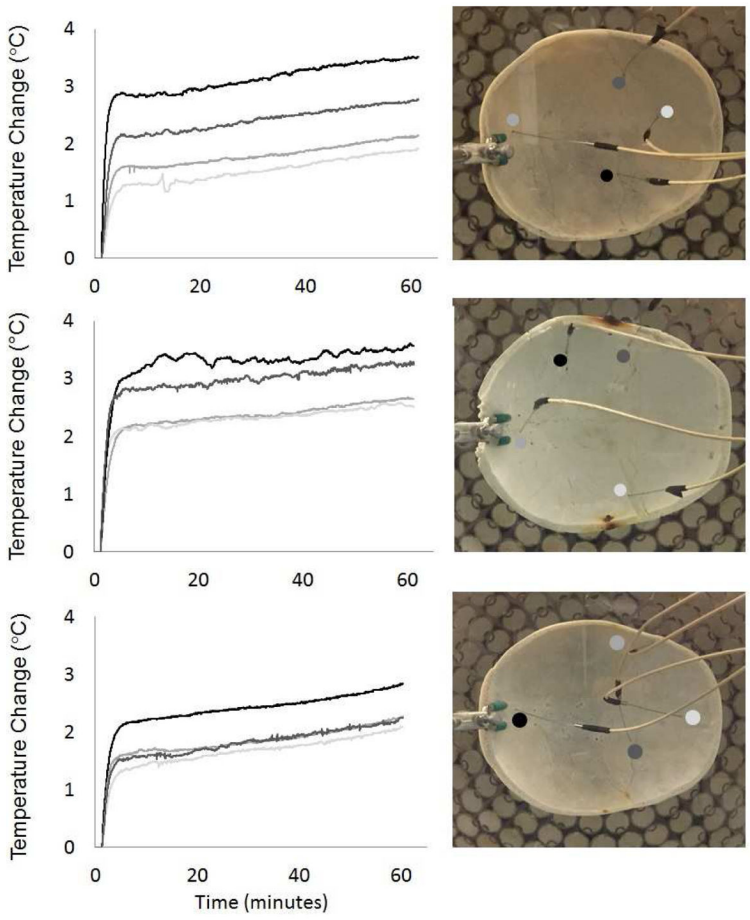


**Figure 10. Skullcap Temperature Monitoring**

The change in temperature in each skullcap monitored at different locations while applying treatment with the 500 kHz array at a PRF of 200 Hz. For each skullcap, the maximum temperature rise remained less than 4 °C. The temperature rise measured by different probes in the skullcaps showed a variation in temperature based on the location of the probe. For skullcaps 1 – 3, the probe measurements varied between 1.9 and 3.5, 2.5 and 3.6 and 2.1 and 2.8 °C, respectively.

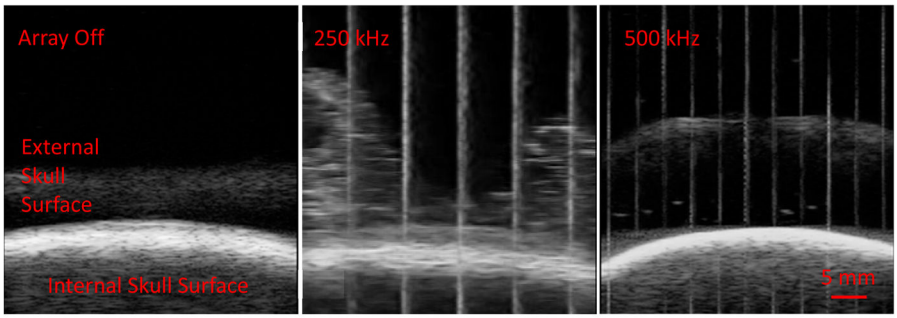


**Figure 11.**
B-mode ultrasound images of external surface of a bleached skullcap during treatment with the 250 and 500 kHz array.

**Table 1**

### Skullcap Characteristics

Table 1 shows the measured dimensions and acoustic properties of the three skullcaps.

| Skull # | Major Dimensions (mm) | | | Thickness (mm) | | | Acoustic Properties | | |
|---|---|---|---|---|---|---|---|---|---|
| | Long Axis | Short Axis | Depth | Min | Max | Mean | 250 kHz Attenuation (dB/cm) | 500 kHz Attenuation (dB/cm) | Sound Speed (m/s) |
| 1 | 161 | 139 | 58 | 2.1 | 8.5 | 5.1 ± 1.3 | 14.4 ± 5.2 | 20.4 ± 6.6 | 2063 ± 402 |
| 2 | 173 | 145 | 63 | 3.7 | 10.4 | 7.0 ± 1.5 | 11.4 ± 4.3 | 11.7 ± 3.4 | 1991 ± 210 |
| 3 | 183 | 143 | 64 | 2.6 | 11.1 | 6.5 ± 1.3 | 14.6 ± 7.7 | 14.5 ± 4.5 | 2340 ± 354 |

**Table 2**

**−6-dB Widths of the Pressure Profiles Measured through the Skullcaps**

Table 1 shows the −6-dB widths of the 1D pressure profiles measured through the three skullcaps.

| | Sagittal (mm) | | Coronal (mm) | | Axial (mm) | |
|---|---|---|---|---|---|---|
| Skull # | 250 kHz | 500 kHz | 250 kHz | 500 kHz | 250 kHz | 500 kHz |
| 1 | 3.7 | 2.0 | 3.2 | 1.8 | 7.6 | 3.8 |
| 2 | 3.7 | 2.0 | 3.2 | 1.7 | 7.0 | 3.6 |
| 3 | 3.4 | 1.9 | 3.2 | 1.8 | 6.9 | 3.5 |

**Table 3**

**Pressure Decrease at Steering Locations Furthest from Geometric Focus through the Skullcaps**

The percentages for the average pressure decrease, across the three skullcaps, at −20 and +20 mm for each axis relative to the geometric focal pressure.

| | Sagittal | | Coronal | | Axial | |
|---|---|---|---|---|---|---|
| **Frequency** | **−20 mm** | **+ 20 mm** | **−20 mm** | **+20 mm** | **−20 mm** | **+20 mm** |
| 250 kHz | 38±4% | 28±4% | 34±2% | 34±3% | 50±1% | 17±2% |
| 500 kHz | 80±7% | 63±4% | 68±4% | 69±7% | 70±5% | 36±3% |

**Table 4**

**P-values for Focal Spacing and Skullcap Comparisons**

The p-values from the two-sample, two-tailed t-tests (α = 0.05) performed on the liquefaction volumes (L.V.) and liquefaction rates (L.R.) between the focal spacing for each skullcap and between the skullcaps for each focal spacing treated at 250 kHz and 500 kHz.

| **250 kHz** | | | | | | | | | |
|---|---|---|---|---|---|---|---|---|---|
| **Spacing:** | | **λ/2 v. 2λ/3** | **λ/2 v. λ** | **2λ/3 v. λ** | **Skull:** | | **1 v. 2** | **1 v. 3** | **2 v. 3** |
| Skull 1 | L.V. | 1.3E-03 | 1.4E-07 | 2.1E-06 | λ/2 | L.V. | 2.4E-04 | 1.9E-04 | 0.53 |
| | L.R. | 4.4E-05 | 2.8E-03 | 9.8E-02 | | L.R. | 2.8E-02 | 0.58 | 3.4E-02 |
| Skull 2 | L.V. | 3.8E-04 | 1.3E-06 | 1.7E-03 | 2λ/3 | L.V. | 1.1E-05 | 4.0E-05 | 0.69 |
| | L.R. | 1.7E-02 | 1.5E-03 | 1.1E-02 | | L.R. | 0.65 | 0.14 | 0.43 |
| Skull 3 | L.V. | 2.8E-02 | 3.3E-04 | 4.8E-05 | λ | L.V. | 7.7E-02 | 0.31 | 0.13 |
| | L.R. | 1.9E-03 | 2.8E-03 | 4.0E-02 | | L.R. | 0.29 | 0.95 | 0.27 |
| 500 kHz | | | | | | | | | |
| Spacing: | | λ/2 v. 2λ/3 | λ/2 v. λ | 2λ/3 v. λ | Skull: | | 1 v. 2 | 1 v. 3 | 2 v. 3 |
| Skull 1 | L.V. | 0.48 | 0.48 | 0.57 | λ/2 | L.V. | 7.0E-05 | 9.0E-05 | 0.50 |
| | L.R. | 3.1E-04 | 4.8E-07 | 1.8E-06 | | L.R. | 2.4E-03 | 1.9E-03 | 0.53 |
| Skull 2 | L.V. | 0.17 | 0.7 | 0.93 | 2λ/3 | L.V. | 4.0E-06 | 3.0E-05 | 0.67 |
| | L.R. | 5.6E-07 | 1.1E-03 | 3.40E-03 | | L.R. | 1.1E-05 | 4.0E-05 | 0.69 |
| Skull 3 | L.V. | 0.41 | 4.1E-04 | 2.6E-04 | Λ | L.V. | 0.13 | 0.29 | 0.18 |
| | L.R. | 9.3E-06 | 5.6E-08 | 1.4E-06 | | L.R. | 7.7E-02 | 0.31 | 0.13 |

## Table 5

### P-values for Frequency Comparisons

The p-values from the two-sample, two-tailed t-tests ($\alpha = 0.05$) performed on the liquefaction volumes (L.V.) and liquefaction rates (L.R.) between 250 and 500 kHz for each focal spacing treated through each skullcap.

| **Spacing:** | | **λ/2** | **2λ/3** | **λ** |
|---|---|---|---|---|
| Skull 1 | L.V. | 2.7E-02 | 2.3E-03 | 3.4E-06 |
| | L.R. | 2.9E-08 | 6.8E-06 | 4.2E-03 |
| Skull 2 | L.V. | 1.5E-03 | 3.9E-07 | 1.3E-02 |
| | L.R. | 8.9E-08 | 1.9E-05 | 2.6E-02 |
| Skull 3 | L.V. | 1.0E-06 | 4.1E-07 | 1.2E-07 |
| | L.R. | 2.7E-05 | 5.3E-06 | 7.3E-03 |